#### RESEARCH PAPER



# Drop-on-demand printed microfluidics device with sensing electrodes using silver and PDMS reactive inks

Avinash Mamidanna<sup>1</sup> · Christopher Lefky<sup>1</sup> · Owen Hildreth<sup>1</sup>

Received: 19 June 2017 / Accepted: 25 October 2017 / Published online: 31 October 2017 © Springer-Verlag GmbH Germany 2017

**Abstract** For this work, a cure-in-place polydimethylsiloxane (PDMS) reactive ink was developed and its utility demonstrated by printing a complete microfluidic mixer with integrated electrodes to measure fluid conductivity, concentration, and mixing completeness. First, a parameter-space investigation was conducted to generate a set of PDMS inks and printing parameters compatible with drop-on-demand (DOD) printing constraints. Next, a microfluidic mixer was fabricated using DOD-printed silver reactive inks, PDMS reactive inks, and a low-temperature polyethylene glycol fugitive ink. Lastly, the device was calibrated and tested using NaCl solutions with concentrations ranging from 0.01 to 1.0 M to show that electrolyte concentration and mixing completeness can be accurately measured. Overall, this work demonstrates a set of reactive inks and processes to fabricate sophisticated microfluidic devices using low-cost inks and DOD printing techniques.

# 1 Introduction

From wax printing of cellulose-based sensors (Lu et al. 2011) to PDMS casting of microfluidic mixers (Li et al. 2014), a number of methods exist to produce microfluidic devices in a rapid manner at affordable costs (Gates et al. 2005; Fuentes and Woolley 2008; Bruzewicz et al. 2008;

**Electronic supplementary material** The online version of this article (https://doi.org/10.1007/s10404-017-2010-8) contains supplementary material, which is available to authorized users.

Xu and Attinger 2008; Comina et al. 2014; Paydar et al. 2014). Although these techniques have advanced the field of microfluidics, a strong discontinuity often exists between the desired device structure (microfluidic path, electronics, chemical sensors, etc.) and the processing strategies needed to fabricate these device structures. For example, paper-based sensors are printed in 2D and then folded into a 3D structure, often with multiple cutting, folding, and taping steps (Bruzewicz et al. 2008; Siegel et al. 2010; Jenkins et al. 2015). Lost-wax and other mold-based processes require master mold fabrication, replication, lithography for electronics, plasma treatments or other adhesion promotion methods, and then final assembly (Zhao et al. 2004; Gates et al. 2004; Cheah et al. 2004). Fully ink-jet printed prototypes of basic microfluidic structures as well as some microfluidics with integrated electronics have also been studied (Su et al. 2016). Unfortunately, most fabrication methods struggle to deposit multiple materials using a single process, and integrating electronics directly into the microfluidic pathway can be extremely challenging.

Drop-on-demand (DOD) printing strategies have a number of benefits over conventional lithography-based fabrication methods (Derby 2010). While more suited for small volume production, DOD printing does not require expensive mask aligners, evaporation or sputtering deposition tools, or etching equipment. Moreover, it avoids hazardous chemicals such as KOH and HF often seen in silicon- and glass-based microfluidic device fabrication. Eliminating photolithography masks also supports rapid iteration and prototyping at low cost. Examples of microfluidic devices fabricated using DOD printing include wax mold microfluidic devices, all-polymer transistor circuit devices, and bioMEMS devices (Sirringhaus et al. 1910; Cooley 2002; Liu et al. 2003). Unlike lithography-based methods, where multiple material layers require careful process planning with limitations



Owen Hildreth owen.hildreth@asu.edu

School for Engineering of Matter, Transport, and Energy, Arizona State University, Tempe, AZ 85287, USA

associated with chemical compatibility between the deposited materials and any etching chemicals, DOD printing is inherently capable of depositing inks of different material compositions (Ibrahim et al. 2006; Li et al. 2009). Additionally, advances in reactive inks are further expanding the utility of DOD printing by enabling the deposition of high-quality materials at low temperatures (< 150 °C). Instead of printing colloidal dispersion of nanoparticles that require high-temperature sintering to achieve reasonable material properties (Chou et al. 2005), reactive inks effectively print chemical reactions. By adjusting ink reaction kinetics and printing parameters, it is possible to print materials with material properties matching those of bulk materials (Walker and Lewis 2012; Rosen et al. 2014; Lefky et al. 2016).

In this work, we introduce a new cure-in-place polydimethylsiloxane (PDMS) reactive ink that enables the buildup of 2.5D PDMS structures directly onto hard substrates. This PDMS reactive ink makes it easy to fabricate active microfluidic devices using DOD printing technologies. First, a parameter-space investigation was conducted to balance print speed and buildup rate with feature resolution and droplet stability. To demonstrate the utility of our PDMS reactive ink, we next printed a complete microfluidic mixing device with integrated sensing electrodes to monitor fluid resistivity, electrolyte concentration, and mixing thoroughness. To fabricate the device, a silver reactive ink was used to print sensing electrodes, and then, the walls of the microfluidic channels were defined using the PDMS reactive ink. Since printing voids using a DOD printer is difficult, the microfluidic channels were filled with a fugitive polyethylene glycol (PEG) ink to act as temporary scaffolding later removed by heating the complete device until the PEG melted and could be pushed clear using water (Shore and Harrison 2005). The immiscibility between the nonpolar PDMS reactive ink and the polar PEG fugitive ink ensured that these layers do not mix and that microfluidic channel could be precisely defined and characterized (van den Berg et al. 2007). It is important to note that, except for a final outer layer added for mechanical stability, the PDMS was not "cast" or molded around the PEG/PEO (polyethylene oxide) and Ag structures as is typically done (Fuentes and Woolley 2008; Thomas et al. 2009). Instead, the microfluidic PDMS pathway was printed using a PDMS ink without any molding steps.

Once the device was fabricated, the cell constant curves for each inlet and outlet were calibrated using NaCl solutions of known concentration and resistivity. Next, 1.0 and 0.01 M NaCl solutions were flown through the left and right inlets, while the electrical resistance at the inlet and outlet sensing electrodes was measured. Using the previous calibrations, the NaCl concentration can be empirically determined, and the effectiveness of the mixing can be monitored in situ as flow rate is varied. Overall, these reactive inks and DOD printing processes enable CAD-to-FAB design strategies where separate components are integrated together seamlessly during the fabrication process.

# 2 Experimental setup

# 2.1 Printing and metrology

All printing was done using a Microfab Jetlab II with precision stage and digital pressure controller. A built-in camera and strobe was used to observe drop formation, droplet diameter, and droplet velocity. Printing parameters, shown in Table 1, were optimized to minimize satellite droplets and maximize droplet stability. Ink viscosity was measured using a Rheosense microVISC HVROC-S. The contact angle between the ink and substrate was periodically measured using a Rame-Hart 290-U1 goniometer to determine whether surface modification using O<sub>2</sub> plasma was necessary to keep the ink wetting on the substrate. All solid chemicals were used as received; liquid chemicals were filtered through either a nylon filter for polar liquids or a polytetrafluoroethylene (PTFE) for nonpolar liquids with a manufacturer-stated pore size of 450 nm.

Salt solutions of NaCl (Sigma-Aldrich, ACS reagent) in  $18 \,\mathrm{M}\Omega\,\mathrm{H}_2\mathrm{O}$  (ELGA, Purelab Flex) of various concentrations were used to test the device's capability as a conductivity meter. As a reference, the conductivity of the salt solutions was measured using a Mettler-Toledo Seven excellence pH/Conductivity meter with iLab 710 conductivity probe. An Agilent U1272A Multimeter was used to monitor the

**Table 1** Printing parameters for inks used to fabricate microfluidic device

Ink	Nozzle dia. (µm)	Sub. temp. (°C)	Pitch (µm)	Rise (fall) (µs)	Dwell (Echo)		Press. (kPa)
					(µs)	(V)	
PDMS	40	130	70	3 (4)	30 (40)	25 (- 25)	- 1.3
PEG	60	70	25	3 (4)	35 (40)	25 (- 25)	- 1.0
Ag	57	90	25	3 (4)	55 (10)	25 (- 25)	- 1.3

Note that the echo time was 0  $\mu$ s for all inks and that the 300 Hz ejection frequency was just for droplet inspection. Printing was done on the fly with print ejection frequency given by nozzle velocity/pitch spacing



resistance of each fluid through both the inlet channels and also the resistance across both the outlet channels after fluid mixing.

# 2.2 Ag reactive ink

Adhesion of silver electrodes to the substrate plays a major role in its functionality as a device. Poor adhesion results in broken electrodes and poor repeatability. A solution of 0.5 M tin (II) chloride solution in 18 M $\Omega$  DI water and 0.5 M HCl was used as a sensitizing agent and adhesion promoter (Wei and Roper 2014). Substrates were dipped in this solution for 300 s and dried using N<sub>2</sub>.

A modified version Lewis' group silver reactive ink solution was used as our silver ink (Walker and Lewis 2012). 2.00 g of silver acetate (C<sub>2</sub>H<sub>3</sub>AgO<sub>2</sub> anhydrous, Alfa Aesar, 99%) was dissolved in 5.00 mL ammonium hydroxide (NH<sub>4</sub>OH, VWR, 28–30 wt% ACS Grade) followed by adding dropwise 0.4 mL formic acid (HCOOH, Sigma-Aldrich, Anhydrous > 96%). The ink was allowed to sit for 12 h under ambient conditions and then filtered through a 450nm nylon/polypropylene filter and stored at 4 °C (fridge temperature) until use. Drop stability and printed silver quality were improved by diluting the base silver ink 1:10 by volume with ethanol (Lefky et al. 2016). The ink solution was filtered one last time immediately prior to printing. Silver electrodes were printed onto a substrate held at 90 °C with a 57-µm orifice diameter nozzle using the jetting parameters listed in Table 1.

## 2.3 PDMS ink

Dow Corning's Sylgard 184 silicone elastomer kit formed the basis of the PDMS ink. Four different combinations of silicone, cyclohexane, and toluene ratios were evaluated for down-selection. Critical parameters for down-selection were jetting stability, droplet velocity (maximized), satellite formation (minimized), droplet evaporation, feature resolution, cure temperature, and cure speed. Ultimately, a base silicone solution consisting of Sylgard 184 Part A and Part B in the manufacturer's recommended 10:1 Part A to Part B (herein called "PDMS") by weight was diluted 1:5 (PDMS/toluene) by volume. The addition of the lower vapor pressure toluene in this ratio ensures jet stability when printing above a substrate held at 130 °C. The jetting parameters for this ink using a 40-µm orifice diameter nozzle are listed in Table 1.

# 2.4 PEO and PEG inks

Various mixtures of PEO, PEG, H<sub>2</sub>O, and ethanol (EtOH) were tested to balance fill rate with jet stability. PEO (10,000 MW), PEG (1305–1595 MW), and EtOH (200 Proof, Anhydrous) were purchased from Sigma-Aldrich

and used as received. 18 M $\Omega$  DI water was used after filtering through a 450-nm nylon/polypropylene filter. Inks were mixed at various weight percentages with the solvents and stirred for 2 min using a magnetic stir bar. Magenta ink (generic colored ink-jet ink) was added to the PEO/PEG inks to aid visualization of the printed device. The inks were filtered one last time prior to printing. "Results and discussion" section details our down-selection process. Ultimately, a solution of 4 wt% PEG in DI water produced stable drops with a fast fill rate as long as an  $O_2$  plasma surface treatment was conducted immediately prior to printing. This ink was printed at a substrate temperature of 70 °C from a 60- $\mu$ m orifice nozzle using the printing parameters listed in Table 1.

#### 2.5 Oxygen plasma treatment

O<sub>2</sub> plasma surface treatments improve PEG ink wetting so that higher PEG concentrations would form continuous lines when printed in the PDMS-defined channels. A small optimization test was used to establish the minimum time and power needed to treat the surface without damaging the substrate and silver electrodes. O<sub>2</sub> plasma treatments were conducted in a Venus 25 Plasma Etch system at 60 W for 10 s.

#### 2.6 Device fabrication

Figure S1 (see Online Resource 1) shows the device fabrication steps. The glass substrate is first treated for 30 s in a low-power O<sub>2</sub> plasma and then immersed for 5 min in the tin (II) chloride sensitizing solution in order to promote adhesion of the Ag electrodes printed on it. Next, 10 layers of Ag ink are printed with the print stage held at 90 °C to form electrodes for sensing conductivity. 1 mm<sup>2</sup> silver pads are printed as shown in Fig. S1 at the ends of the silver electrodes to serve as probing pads for electrical resistance measurements. 50-75 layers of PDMS of the desired geometry with zigzag interlinks to provide a turbulent fluid flow pathway are printed with the print stage held at 130 °C, forming a PDMS channel to confine subsequent PEG inks. This channel increases both the lateral resolution of the microfluidic and the vertical height; without this channel, the PEG spreads out into a wide, thin film that limits the density of microfluidic lines while increasing confinement drag. Immediately prior to PEG filler printing, the PDMS and glass surfaces were treated by an O<sub>2</sub> plasma to increase the wettability of polar PEG inks on PDMS and improve the continuity of PEG polymer fillers. The device is masked before plasma treatment such that only the PDMS is exposed to the plasma and the silver remains unaffected (to prevent oxidation of silver).

One thousand layers of PEG 4 wt% in water were printed onto the substrate held at 70 °C. The sample is then cooled to room temperature to solidify the polymer filler. Following



this, a pure elastomeric mold of the Sylgard 184 is created and glued onto the glass substrate around the device to act as a confinement wall for the PDMS cap. Undiluted PDMS is then poured over the device and cured at 40 °C for 12 h to seal the device completely. This thicker PDMS layer was necessary to physically hold the inlet and outlet ports without tearing. A 1.5-mm-diameter biopsy punch is used to punch holes through the top PDMS confinement to make the inlet and outlet ports. Lastly, the polymer filler is removed by heating the device on a hot plate held at 60 °C and flowing red-dyed- and blue-dyed water at the same rates through two inlet ports simultaneously. The flow pressure is controlled and adjusted using an Elveflow OB1 MK3 pressure controller such that mixing of the two fluids occurs across the channel.

## 3 Results and discussion

# 3.1 Optimization of PDMS inks

The parameters for stable, satellite-free droplets vary with local ambient conditions, such as humidity and temperature. An investigation of solvents with different vapor pressures was performed to establish PDMS inks that would be stable over long print times. Initially, we tested cyclohexane as the solvent for PDMS inks; however, this ink was only stable for short print times of 5–10 min before the nozzle would dry out. Next, various mixtures of cyclohexane and toluene were tested for jet stability and feature resolution and a PDMS ink of 1:5—PDMS/toluene was chosen due to its long-term print stability (> 2 h) and reasonable line width (200–300 µm) when printed from a 40-µm nozzle onto a heated substrate.

The optical images in Fig. 1 show a small optimization study of the PDMS ink for three different substrate temperatures and droplet spacings. As expected, lowering pitch increases droplet overlap and increases line width. Increasing substrate temperature drives off excess solvent faster and increases the PDMS cure rate, resulting in smaller line widths. The ideal droplet spacing and temperature to obtain a PDMS line that is both cured and has minimal droplet spreading are 70 microns. For device fabrication, we settled on a droplet spacing of 70  $\mu$ m and a substrate temperature of 130 °C because it balanced the high-feature resolution seen at 150 °C with the droplet stability seen at 120 °C.

# 3.2 Device fabrication and testing

#### 3.2.1 Fabrication

Device fabrication is schematically illustrated in Fig. S1 and described in detail in the experimental methods. The printing process begins by first cleaning the glass substrate and depositing a tin adhesion layer. Next, a set of Ag electrodes are printed using reactive silver ink at 90 °C, and then, the PDMS geometry is printed using a reactive PDMS ink at 130 °C to help confine subsequent PEG layers. The 4 wt% PEG fugitive phase changing ink is printed at 70 °C, filling the PDMS dam.

Figure 2a shows a top-down optical image of a section of the mixing channel after printing 1000 PEG layers, and Fig. 2b shows the mixing channel after being capped. These representative images demonstrate that the fugitive PEO ink forms a continuous structure confined by the PDMS channels throughout the entire device. While 1000 layers sounds like a lot, each layer was actually printed as a straight line

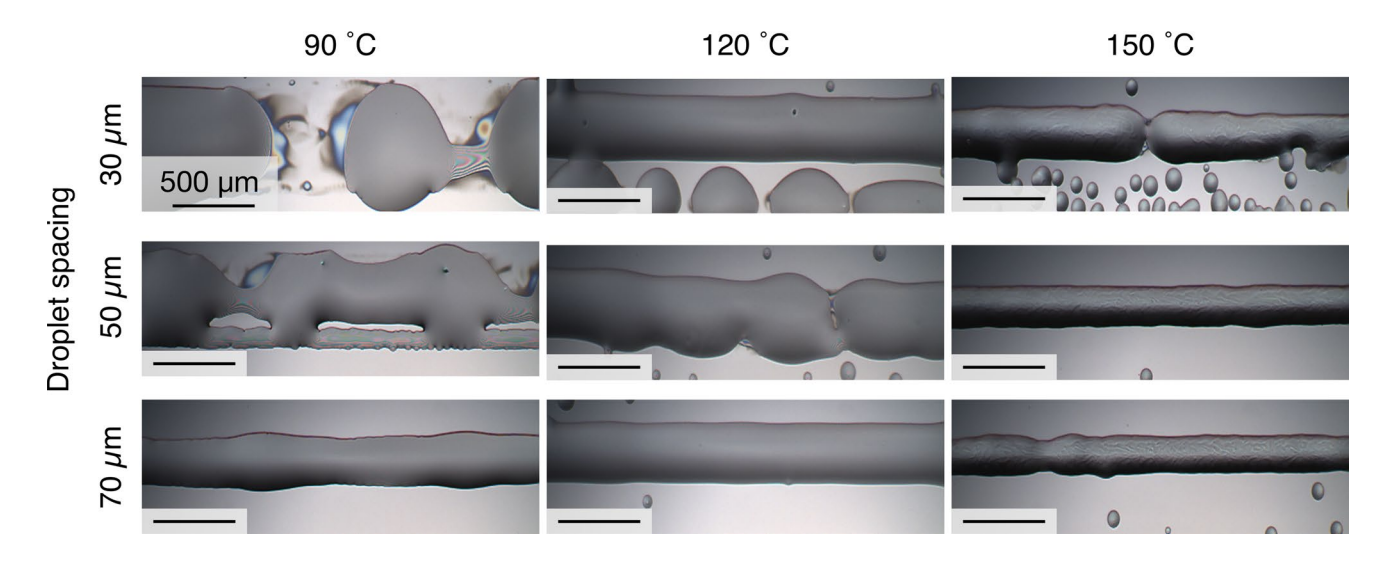


Fig. 1 Parameter-space investigation of droplet pitch versus substrate temperature. The final device was printed using 70-μm pitch with the substrate held at 130 °C to balance feature resolution and droplet stability



Fig. 2 Optical top-down images of mixer microchannel after PEG filler material printing a before capping it with PDMS and b after capping it with PDMS

instead of following the curving microfluidic path. This straight-line approach was simple to implement, minimized layer print time, and reduced the chance of stray PEG droplets landing outside of the PDMS channel. Thickness of the PEG layer was measured at 130 µm using a Dektak contact profilometer (see Online Resource 1). Figure 3a shows the final device before PDMS encapsulation with 1 mm<sup>2</sup> silver pads printed at the end of the silver electrodes to act as a landing pad for the 2-point resistance probes.

A number of approaches were explored to physically connect the printed microfluidic device to the OB1 MK3 microfluidics controller. We settled on casting a thicker layer of PDMS on top of the printed device to create a mechanically robust interface with little effort. A pure elastomeric "ring" of undiluted PDMS was cast into a mold printed using a CubePro filament 3D printer. As shown in Fig. 3b, this ring was placed around the device and attached to the glass substrate using more PDMS. Next, additional undiluted PDMS was poured into this ring, over the device, and then cured at 40 °C for 12 h to seal the device completely in a mechanically robust manner. A 1.5-mm-diameter biopsy punch is used to punch holes through the PDMS encapsulant to make the inlet and outlet ports. The two inlet ports were connected to a dual-channel Elveflow OB1 MK3 pressuredriven microfluidics controller with an in-line flow meter for independent feedback control. The polymer filler is removed by heating the device on a hot plate held at 60 °C and flowing red-dyed and blue-dyed water through two inlet ports simultaneously (see Fig. 3c).

# 3.2.2 Testing the microfluidic mixer

The mixing of the fluids in the microfluidic channel is dependent on the fluid flow Reynolds number,  $Re = \rho \nu L / \mu$ , where  $\rho$  is the fluid density,  $\nu$  is the fluid velocity, L is the characteristic length (channel height in this case), and  $\mu$  is the fluid viscosity. The Reynolds number versus flow rate was calculated for the microchannel assuming no zigzag features. This preliminary calculation showed us that a more tortuous geometry would need to be present to induce

turbulence in the fluid flow and facilitate mixing. This work was partly inspired by (Mengeaud et al. 2002) who presented finite element simulations on zigzag microchannels to show that using the zigzag configuration, a hydrodynamic phenomenon known as laminar recirculation contributed to mixing. The mixing of fluids in the microchannel improved due to the inertial effects at the angles leading to a boundary-layer separation corresponding to the inversion of pressure gradient and wall shear stress. A number of trial experiments were conducted to balance the number of printed PEG layers to achieve mixing while still maintaining a reasonable print time (see Online Resource 1). Ultimately, we settled on 1000 layers of PEG 4 wt% in water printed onto the substrate held at 70 °C. This yielded a channel height of 130 µm as measured using a Dektak profilometer (see Online Resource 1).

The fluid sensor connected to the OB1 digital pressure controller could only measure flow rates up to  $80 \,\mu\text{L/min}$ ; data on pressure versus flow rate for our microfluidic device were collected and fit using a linear fit so that flow rates at higher driving pressures could be estimated. Figure 4 shows this flow rate versus pressure data along with the extrapolated fit to of  $410 \,\mu\text{L/min}$  at  $400 \,\text{mbar}$ .

Next, salt solutions of NaCl/ $H_2O$  of different concentrations (1, 0.5, 0.1, 0.05, 0.01 M) were prepared, and their standard resistivity values were obtained from a Mettler-Toledo Seven Excellence pH/conductivity meter. To each solution, a blue or red dye pigment was added alternately such that two solutions being flown through the mixer device at any time had two different colors. Solutions of every concentration were flown through both the inlet channels to account for the cells geometric correction factor. Resistance values were recorded across all ports for all combinations of electrolyte concentration mixing.

Figure 5a shows 1 M NaCl (blue) and 0.01 M NaCl (red) solutions flowing at 80  $\mu$ l/min. It is evident that no mixing occurs at this flow rate because a clear delineation between the red and blue fluids is observed. In Fig. 5b, however, the driving pressure is increased to 400 mbar for each channel for an estimated flow rate (Q) of 410  $\mu$ L/min. The fluids appear to completely mix at this high flow rate and the



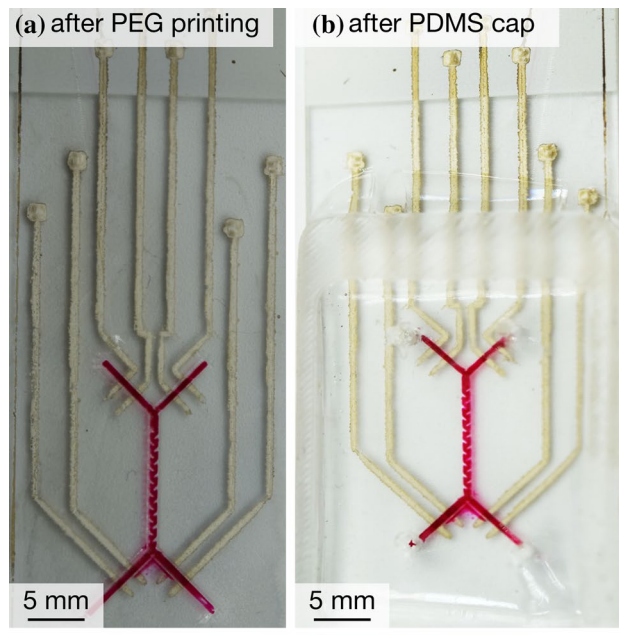




**Fig. 3** Microfluidic mixer device with PDMS channel confining 1000 layers of the PEG filler material with the silver sensing electrodes before capping the device with the top layer PDMS

output channels appear as greyish purple. However, visual inspection is not a precise or quantitative method of determining mixing completeness.

To illustrate the utility of DOD printing of reactive inks, the silver electrodes printed directly into the fluid pathway allows us to directly measure the resistivity of the incoming and outgoing fluids so that the final concentrations at the output ports can be measured. First, the fluid resistivity of NaCl solutions,  $\rho$ , at various concentrations was measured using a Mettler-Toledo InLab Power Pro with an iLab 710

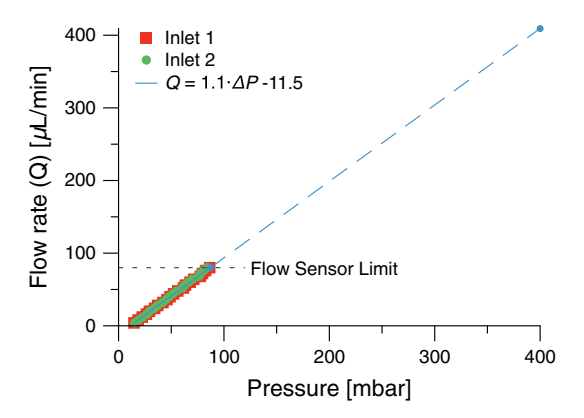


**Fig. 4** Plot for flow rate versus applied pressure through the Inlets 1 and 2. Since the flow sensor used in this study had a limit of  $80~\mu\text{L/min}$ , a linear fit (blue dashed line) of measured values was used to extrapolate the flow rate of 410  $\mu\text{L/min}$  at 400 mbar (color figure online)

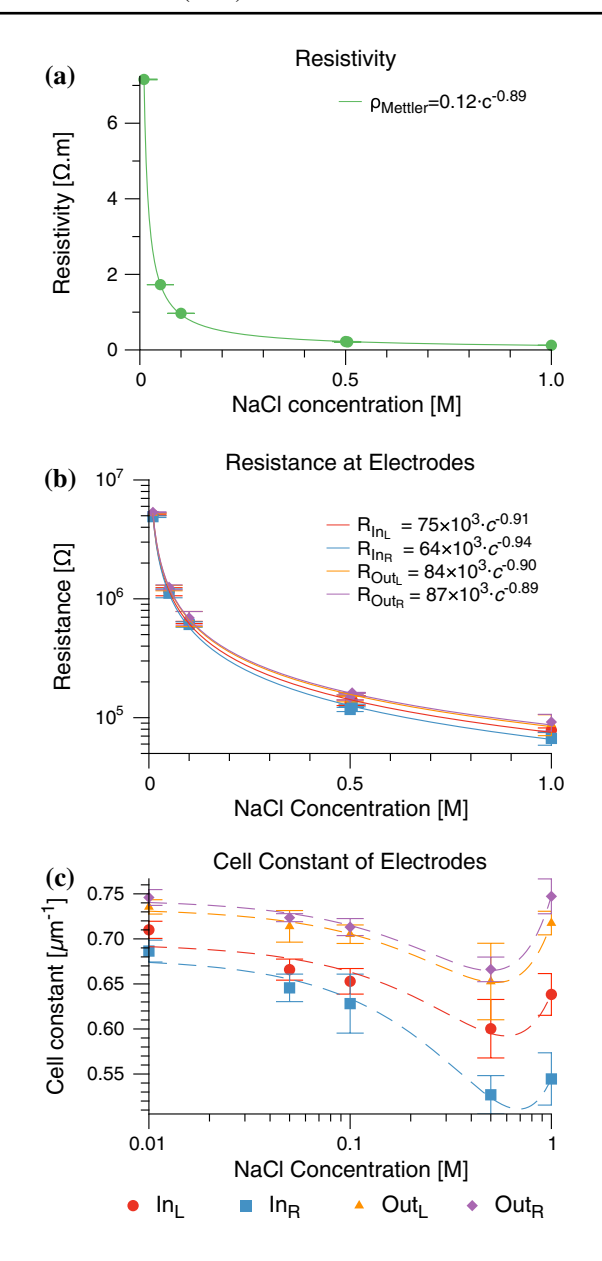


Fig. 5 Optical top-down images of the microfluidic mixer channel near outlets ports during flushing  ${\bf a}$  no mixing occurs between the blue NaCl 1 M solution and red NaCl 0.01 M solution flowing at 80  $\mu$ l/min and  ${\bf b}$  complete mixing appears to occur at 410  $\mu$ l/min (color figure online)

conductivity probe. These data are plotted in Fig. 6a and fit using a power law as  $\rho = 0.12 \cdot c^{-0.89}$  [ $\Omega$  m]where c is the NaCl concentration (Godwin et al. 2013).

Next, the concentration dependence of the resistance of each inlet and outlet probe was established at 410  $\mu$ L/min. Figure 6b plots the resistance versus NaCl concentration ( $R_{\rm conc.}$ ) at the inlets and outlets and fitted using a power law. Notice that there is some deviation in the exponent between the resistivity fit of the NaCl solutions and the resistance fits. This difference arises because the Mettler-Toledo system





**Fig. 6** Graphs of **a** resistivity of the NaCl solutions used in this set of experiments measured using a Mettler-Toledo conductivity probe; **b** measured resistance at the inlets and outlets; **c** calculated cell constant, C. Notice that C varies with NaCl concentration due to DC polarization (Randall and Scott 2001). From legend, left inlet = red, filled circle; right inlet = blue, filled square; left outlet = orange, filled triangle; right outlet = purple filled diamond (color figure online)

applies an AC signal to filter out the polarization that occurs at the electrodes. The simple 2-point DC resistance measurement used in our microfluidic device does not filter out this polarization effect (Cetin 1997). However, the results should be accurate enough for most applications.

Using a simplified model of  $R = C \cdot \rho$  [ $\Omega$ ], a cell constant, C, connects the measure resistance, R [ $\Omega$ ], to the fluid resistivity. Figure 6c plots the variation in C with NaCl

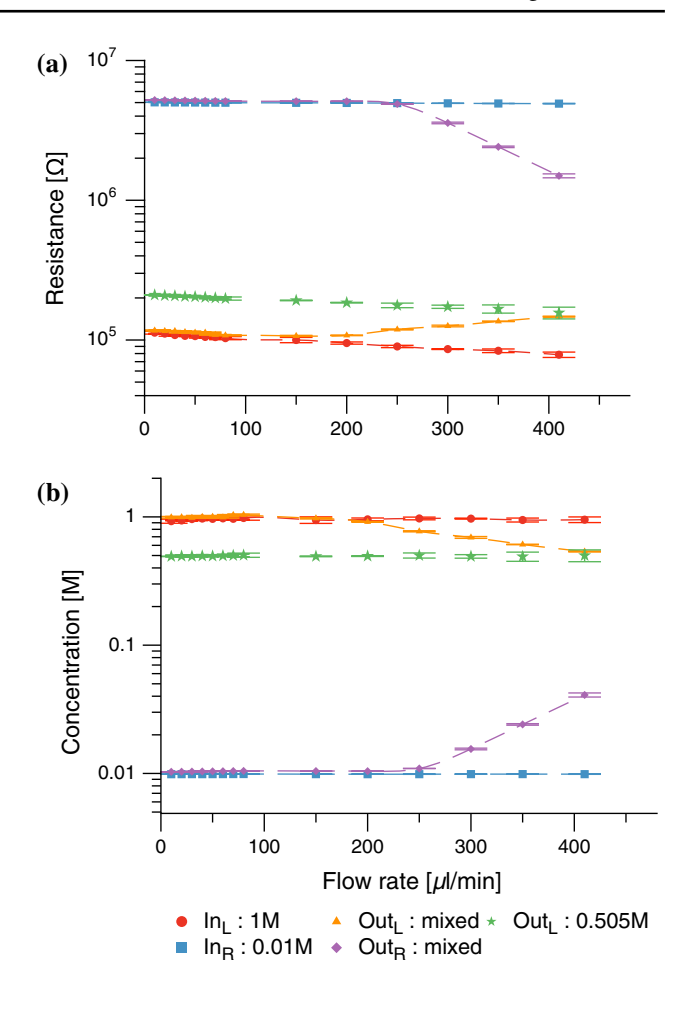


**Fig. 7 a** Measured resistance and **b** calculated concentration at inlet and outlets at flow rates from 10 to 410  $\mu L/min$  with NaCl concentrations for the left and right set of ports set to 0.01 and 1 M, respectively. Additionally, a fully mixed solution 0.505 M NaCl was measured at the left outlet (green, filled asterisk). Notice that the onset of detectable mixing is different between the left and right outlets (200 and 250  $\mu L/min$ , respectively) as is the degree of mixing at 410  $\mu L/min$ . This indicates that the mixing is not complete across microfluidic channel (color figure online)

concentration. The fitted C curves follow the expected shape with the C slowly decreasing with increasing salt concentration and then increasing sharply around 1 M (Randall and Scott 2001). This indicates that, once calibrated to a specific electrolyte and flow rate, the electrolyte concentration at the inlets and outlets could be reasonably determined across three orders of magnitude even if polarization occurs at the electrodes.

Figure 7a plots the measured 2-point DC resistance at each inlet and outlet as flow increases from 10 to 410  $\mu$ L/min with the left and right inlet concentration set to 0.01 and 1.0 M, respectively. As expected, the resistance at the inlets decreases linearly with increasing flow rates even though the inlet concentrations remain constant, while the outlets start out linearly and then deviate at the higher flow rates.



The shift in resistance as a function of flow rate,  $\Delta R_{\rm flow}$ , for each inlet and outlet channel was calculated using the linear portion of these curves at low flow rates below 80  $\mu$ L/min.

Since the  $R_{\rm conc.}$  curves were collected at 410 µL/min, the measured resistance,  $R_{\text{meas}}$  [ $\Omega$ ], was modeled as  $R_{\rm meas.}=R_{\rm conc}+\Delta R_{\rm flow}$ . Using inlet one as an example,  $R_{\rm conc.}=75\times 10^3 \cdot c^{-0.91}~[\Omega]$  and  $\Delta R_{\rm flow}=81.1(f-410)~[\Omega]$ , the concentration at each flow rate can be calculated as: c=  $[75 \times 10^3/(R_{\text{meas.}} - \Delta R_{\text{flow}})]^{-0.91}$  (see Online Resource 2). Appling this process to all inlets and outlets, the calculated concentration versus flow rate is plotted in Fig. 7b. These curves show that the onset of detectable mixing is different between the left and right outlets (200 and 250 µL/min, respectively) as is the degree of mixing at 410 µL/min. It is important to acknowledge that higher flow rates were not tested because the PDMS was found to delaminate from the underlying glass substrate at higher pressures. PDMS adhesion is one limitation with our process that we did not find a perfect solution for. As our PDMS is directly printed onto the glass substrate; we could not take advantage of the O<sub>2</sub> plasma treatment typically used in cast PDMS microfluidic devices. Despite this limitation, this work goes to show that some of the major challenges of a typical LOC fabrication process, such as excessive fabrication costs and difficulty in integration of different microfluidic sub-systems together (Abgrall and Gué 2007), are addressed by this technique. Visually, the fluids appeared fully mixed but the electrical data clearly indicate that the mixing not only is incomplete, but differs between the left and right sides.

By using reactive ink chemistries and DOD printing, it is possible to seamlessly integrate electronic sensing capabilities directly into the microfluidic pathway during the printing process. Additionally, the flexibility of DOD printing means that designs can be updated as often as needed to improve device performance, and DOD techniques have higher throughput with lower production cost per cell when compared to typical LOC techniques (Jenkins et al. 2015).

# 4 Conclusion

In conclusion, we demonstrated a simple process to fabricate a complete microfluidic mixer device, including fluid path and sensing electrodes, using drop-on-demand printing and reactive inks. Su et al. recently described an interesting method of fabricating microfluidics for sensing applications using ink-jet printing; however, the inks used in all their processes needed an additional post-annealing step which makes the entire fabrication process time-consuming (Su et al. 2016). In our process, we could directly print reactive inks onto heated substrates to get solid features without the need for any additional post-annealing steps. Ag electrodes were directly printed and incorporated into the microfluidic

device using self-reducing Ag ink and served to measure fluid resistivity and concentration. A parameter-space investigation for PDMS ink demonstrated a print-stable PDMS ink designed to cure in-place when printed on a substrate held at 130 °C. This PDMS ink has reasonable feature resolution and buildup. A fugitive PEG filler ink was developed to be solid at slightly elevated temperatures yet have reasonably low viscosities at 70 °C so that a fluid pathway can be created by displacing the PEG with water. The device was calibrated by establishing the cell factors to measure fluid resistivity and concentration for salt solutions of different concentrations as well as mixed electrolyte solutions by monitoring 2-point resistance as a function of NaCl concentration. Unlike paper-based microfluidic devices often fabricated using printers, our process demonstrates that flushable, "hard" microfluidic devices can be fabricated using dropon-demand printing. This process should facilitate low-cost microfluidic prototyping and fabrication.

**Acknowledgements** The authors would like to acknowledge the generous support from the National Science Foundation (NSF #1635548) and the Science Foundation Arizona (BSP 0615-15).

### References

Abgrall P, Gué A-M (2007) Lab-on-chip technologies: making a microfluidic network and coupling it into a complete microsystem—a review. J Micromech Microeng 17:R15–R49. https://doi.org/10.1088/0960-1317/17/5/R01

Bruzewicz DA, Reches M, Whitesides GM (2008) Low-cost printing of poly(dimethylsiloxane) barriers to define microchannels in paper. Anal Chem 80:3387–3392. https://doi.org/10.1021/ac702605a

Cetin M (1997) Electrolytic conductivity, Debye-Hu" ckel theory, and the Onsager limiting law. Phys Rev E 55:2814–2817

Cheah CM, Chua CK, Lee CW et al (2004) Rapid prototyping and tooling techniques: a review of applications for rapid investment casting. Int J Adv Manuf Technol 25:308–320. https://doi.org/10.1007/s00170-003-1840-6

Chou K-S, Huang K-C, Lee H-H (2005) Fabrication and sintering effect on the morphologies and conductivity of nano-Ag particle films by the spin coating method. Nanotechnology 16:779–784. https:// doi.org/10.1088/0957-4484/16/6/027

Comina G, Suska A, Filippini D (2014) PDMS lab-on-a-chip fabrication using 3D printed templates. Lab Chip 14:424–430. https://doi.org/10.1039/C3LC50956G

Cooley P (2002) Applications of ink-jet printing technology to bioMEMS and microfluidic systems. J Assoc Lab Autom 7:33–39. https://doi.org/10.1016/S1535-5535(04)00214-X

Derby B (2010) Inkjet printing of functional and structural materials: fluid property requirements, feature stability, and resolution. Ann Rev Mater Res 40:395–414. https://doi.org/10.1146/annurev-matsci-070909-104502

Fuentes HV, Woolley AT (2008) Phase-changing sacrificial layer fabrication of multilayer polymer microfluidic devices. Anal Chem 80:333–339. https://doi.org/10.1021/ac7017475

Gates BD, Xu Q, Love JC et al (2004) Unconventional fabrication. Ann Rev Mater Res 34:339–372. https://doi.org/10.1146/annurev.matsci.34.052803.091100



- Gates BD, Xu Q, Stewart M et al (2005) New approaches to nanofabrication: molding, printing, and other techniques. Chem Rev 105:1171–1196. https://doi.org/10.1021/cr0300760
- Godwin LA, Deal KS, Hoepfner LD et al (2013) Measurement of microchannel fluidic resistance with a standard voltage meter. Anal Chim Acta 758:101–107. https://doi.org/10.1016/j. aca.2012.10.043
- Ibrahim M, Otsubo T, Narahara H et al (2006) Inkjet printing resolution study for multi-material rapid prototyping. JSME Int J Ser C Mech Syst Mach Elem Manuf 49:353–360
- Jenkins G, Wang Y, Xie YL et al (2015) Printed electronics integrated with paper-based microfluidics: new methodologies for next-generation health care. Microfluid Nanofluid. https://doi.org/10.1007/ s10404-014-1496-6
- Lefky C, Mamidanna A, Huang Y, Hildreth O (2016) Impact of solvent selection and temperature on porosity and resistance of printed self-reducing silver inks. Phys Status Solidi A 213:2751–2758. https://doi.org/10.1002/pssa.201600150
- Li L, Saedan M, Feng W et al (2009) Development of a multi-nozzle drop-on-demand system for multi-material dispensing. J Mater Process Technol 209:4444–4448. https://doi.org/10.1016/j.jmatprotec.2008.10.040
- Li Z, Hou L, Zhang W, Zhu L (2014) Preparation of PDMS microfluidic devices based on drop-on-demand generation of wax molds. Anal Methods 6:4716–4717. https://doi.org/10.1039/c4ay00798k
- Liu Y, Cui T, Varahramyan K (2003) All-polymer capacitor fabricated with inkjet printing technique. Solid-State Electron 47:1543– 1548. https://doi.org/10.1016/S0038-1101(03)00082-0
- Lu Y, Lin B, Qin J (2011) Patterned paper as a low-cost, flexible substrate for rapid prototyping of PDMS microdevices via "liquid molding". Anal Chem 83:1830–1835. https://doi.org/10.1021/ac102577n
- Mengeaud V, Josserand J, Girault HH (2002) Mixing processes in a zigzag microchannel: finite element simulations and optical study. Anal Chem 74:4279–4286. https://doi.org/10.1021/ac025642e
- Paydar OH, Paredes CN, Hwang Y et al (2014) Characterization of 3D-printed microfluidic chip interconnects with integrated O-rings. Sens Actuators A 205:199–203. https://doi.org/10.1016/j.sna.2013.11.005

- Randall M, Scott GN (2001) The variation of the cell constant with concentration and the molal conductance of aqueous barium nitrate, sodium sulfate and sulfuric acid at 0'. J AM Chem Soc 49:636–647
- Rosen Y, Grouchko M, Magdassi S (2014) Printing a self-reducing copper precursor on 2D and 3D objects to yield copper patterns with 50% copper's bulk conductivity. Adv Mater Interfaces 2:n/a-n/a. https://doi.org/10.1002/admi.201400448
- Shore HJ, Harrison GM (2005) The effect of added polymers on the formation of drops ejected from a nozzle. Phys Fluids 17:033104–033108. https://doi.org/10.1063/1.1850431
- Siegel AC, Phillips ST, Dickey MD et al (2010) Foldable printed circuit boards on paper substrates. Adv Funct Mater 20:28–35. https:// doi.org/10.1002/adfm.200901363
- Sirringhaus H, Kawase T, Friend RH et al (1910) High-resolution inkjet printing of all-polymer transistor circuits. Science 290:2123–2126
- Su W, Cook BS, Fang Y, Tentzeris MM (2016) Fully inkjet-printed microfluidics: a solution to low-cost rapid three-dimensional microfluidics fabrication with numerous electrical and sensing applications. Sci Rep 6:35111. https://doi.org/10.1038/srep35111
- Thomas MS, Millare B, Clift JM et al (2009) Print-and-peel fabrication for microfluidics: what's in it for biomedical applications? Ann Biomed Eng 38:21–32. https://doi.org/10.1007/s10439-009-9831-x
- van den Berg AMJ, de Laat AWM, Smith PJ et al (2007) Geometric control of inkjet printed features using a gelating polymer. J Mater Chem 17:677–683. https://doi.org/10.1039/B612158F
- Walker SB, Lewis JA (2012) Reactive silver inks for patterning high-conductivity features at mild temperatures. J Am Chem Soc 134:1419–1421. https://doi.org/10.1021/ja209267c
- Wei X, Roper DK (2014) Tin sensitization for electroless plating review. J Electrochem Soc 161:D235–D242. https://doi.org/10.1149/2.047405jes
- Xu J, Attinger D (2008) Drop on demand in a microfluidic chip. J Micromech Microeng 18:065020. https://doi.org/10.1088/0960-1317/18/6/065020
- Zhao X-M, Xia Y, Whitesides GM (2004) Fabrication of three-dimensional micro-structures: microtransfer molding. Adv Mater 8:837–840

